A Wide-Input High Step-Up Resonant Converter With High-Ratio Transformer in High-Voltage Applications

Yuge Yue, Guangzhu Wang, *Member, IEEE*, and Wenjie Guo

***Abstract*—This article uses a transformer and a resonant network to present an isolated dc/dc resonant converter with a step-up ratio of tens to hundreds of times. The transformer leakage inductance replaces the resonant inductor, and the integration of the transformer and the resonant network is realized. The step-up frequency characteristics of the resonant network are analyzed in detail, and the operating range for soft-switching is given. Analyzing the power characteristics shows that it is very suitable for wind power conversion and high-voltage dc collection applications. The optimal design method between transformer ratio and resonant network step-up ratio is given. A 3000 W experimental prototype operating at 46 V/3000 V is built to verify the analysis and performance of the proposed converter. The results show that the step-up ratio of 65-278 is achieved in the output power range of 3000-500 W, with the maximum efficiency reaching 97.4% .**

***Index Terms*—DC/DC converter, high-gain converter, resonant network, soft-switching.**

I. Introduction

With the rapid growth of new energy generation capacity such as wind and solar energy, traditional ac grid connection, and transmission face many challenges due to their intermittency and randomness [1]. DC collection and dc transmission are recognized as the most effective technical solution and inevitable trend to solve the flexible access of large-scale, long-distance wind, solar, and other new energy generation. Constructing a high-voltage flexible dc power grid is necessary to promote the use of new energy sources [2]. Currently, the promising parallel networking in dc collection [3] includes the two-stage step-up type, low-voltage collection centralized step-up type, and single-stage step-up type, as shown in Fig. 1. The single-stage step-up type uses high-voltage collection with lower power loss, eliminates the large dc/dc converter station platform, and meets the power capacity of a single wind turbine. However,

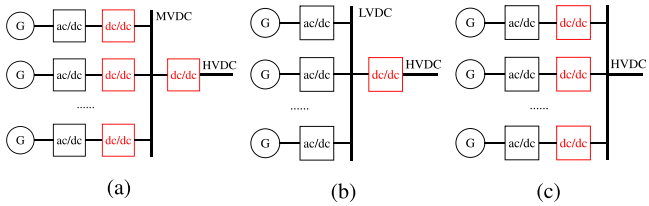

Fig. 1. Structure for connecting multiple DC wind farms in a parallel network for DC transmission. (a) Two-stage step-up type. (b) Low-voltage collection, centralized step-up type. (c) Single-stage step-up type.

the total voltage step-up ratio reaching tens to hundreds of times is one of the major challenges in dc/dc conversion.

The topology of step-up large-capacity dc/dc converters [4] evaluated in numerous studies can be categorized into nonisolated converters, such as the resonant converters based on thyristors [5], the resonant switched capacitor converters [6], dc/dc modular multilevel converters (MMC) [7], isolated converters that mainly comprises traditional full-bridge converters [8], [9], and dual active bridge converters, MMC isolated converters [10]. They usually rely on the cascade of multiple modules or submodules to realize high-voltage power conversion at a high cost and low efficiency.

Recently, step-up resonant converters received more attention due to their wide operating range, low cost, and soft-switching features consisting of zero-voltage switching (ZVS) and zero current switching (ZCS) [11], [12]. They have higher efficiency, and the step-up ratio can be achieved more than 10 times [13], [14], [15]. Thus, the resonant converter is suitable for many step-up applications, such as photovoltaic (PV) systems [16], [17], electric vehicles (EV) charging [18], and dc collection systems [19].

A series resonant dc/dc converter with a wide operating range is proposed in [20]. The converter suits the dc/dc stage of grid-connected PV systems well, with a high efficiency due to the resonant network. A step-up converter for a dc collection system is proposed in [21], however, the auxiliary switches and transformer are used. Abbasi and Lam [22] proposed a modular step-up dc/dc converter with magnetically integrated voltage doublers that can be utilized in a medium-voltage dc grid, achieving a high step-up ratio and power rate. They propose a hybrid high voltage gain converter module for medium voltage dc conversion in [23] soon afterward. This converter achieves

Received 15 March 2025; revised 3 May 2025; accepted 9 June 2025. Date of publication 12 June 2025; date of current version 5 August 2025. This work was supported in part by the National Natural Science Foundation of China under Grant 52177183 and in part by the Key Program of Joint Fund for Regional Innovative Development of the National Natural Science Foundation of China, under Grant U23A20654. Recommended for publication by Associate Editor F. Azcondo. *(Corresponding author: Guangzhu Wang.)*

The authors are with the School of Electrical Engineering, Shandong University, Jinan 250061, China (e-mail: yueyuge@mail.sdu.edu.cn; sdwgz@sdu.edu.cn; 202114550@mail.sdu.edu.cn).

Color versions of one or more figures in this article are available at https://doi.org/10.1109/TPEL.2025.3579118.

Digital Object Identifier 10.1109/TPEL.2025.3579118

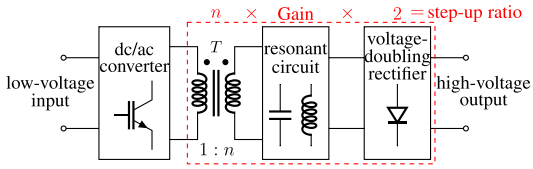

Fig. 2. Design mentality of the proposed converter.

a very high efficiency and a high step-up ratio. However, the step-up ratio of each module is not very high because the step-up ratios of the transformer and resonant network are not distributed perfectly.

However, few existing methods mention the special circumstances with high-voltage transformers. The large turns and insulation structure cause the leakage inductance to be too large, shortening the voltage regulation ability of the converters. The classical design methods may not benefit the cooperation of the transformer and resonant network, limiting the improvement of the step-up ratio. Besides, the special soft-switching and gain characteristics of the resonant converters when operating in the high-gain region are less mentioned in the existing papers, which is necessary for a high step-up and wide-range operation. Furthermore, few existing resonant converters consider the cooperation of the transformer and resonant network and reach a step-up ratio of hundreds of times.

In this article, the main contribution is to investigate the ability of the resonant network further, search for a method to overcome the inherent shortcomings of the undesired large leakage inductance, realize the step-up potential of the resonant tank, and enhance the coordination of the transformer and resonant network. Thus, this article intends to "multiply" the multistage step-up units in a single resonant structure to further enhance the step-up ability of the resonant converter, as illustrated in Fig. 2.

The rest of this article is organized as follows. Section II provides the step-up converter. Section III introduces the design and optimization method. A prototype and the experimental results are presented in Section IV. Finally, Section V concludes this article.

II. Proposed High Step-Up Converter

A. Selection of Resonant Network

The transformer is inevitable in a resonant converter to ensure isolation and provide a ratio n. As shown in Fig. 3(a), most transformers with compact structures are used in resonant converters, and magnetic integration is a popular method to provide resonant parameters by design. However, to enhance insulation, the separated winding shown in Fig. 3(c) is preferred in high-voltage transformers, and the energy distribution shown in Fig. 3(d) is much wider than that shown in Fig. 3(b). This structure reduces the primary-to-secondary interactions while resulting in a significant leakage inductance, whose equivalent circuit model is shown in Fig. 4. Thus, the traditional design method is constrained because transformer manufacturing may not permit an arbitrary turns ratio with the desired leakage inductance. Besides, the series inductance is detrimental to the step-up

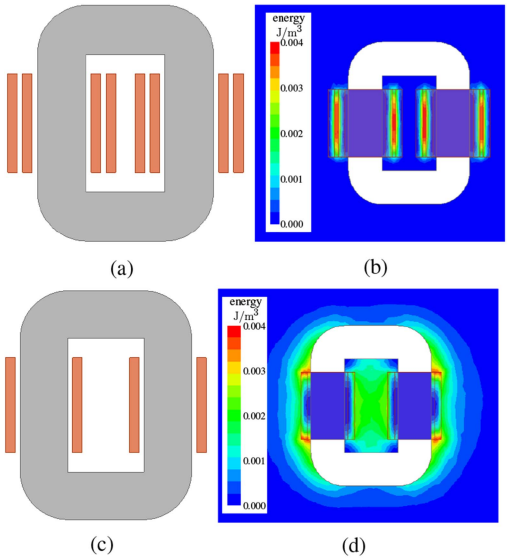

Fig. 3. Transformer structure and magnetic field energy distribution. (a) Transformer with a concentric winding structure. (b) Energy distribution of the concentric winding structure. (c) Transformer with a separated winding structure. (d) Energy distribution of the separated winding structure.

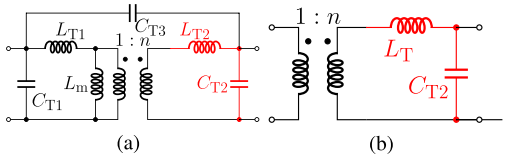

Fig. 4. Equivalent circuit model of the transformer. (a) Equivalent circuit model. (b) Simplified equivalent circuit model.

ratio for many resonant converters, such as the commonly used *LLC* resonant converter, bringing difficulties in the conventional magnetic integration design. The traditionally used inductance serving the resonant network now becomes a hindrance, which needs to be handled in turn.

Due to the high ratio, the leakage inductance is equivalent to the secondary side, and the resonant network is on the output side. The output stage utilizes voltage-doubling half-wave rectification, whose center point is directly grounded with the lower end of the secondary side for insulation. Considering the gain of the resonant network is G, and the input and output voltage are V_{i} and V_{o}, the total step-up ratio is

$$k_{\mathrm{boost}} = \frac{V_{\mathrm{o}}}{V_{\mathrm{i}}} = 2nG. \tag{1}$$

A step-up *LC* parallel resonant network can be used to overcome the adverse effects brought by the large leakage inductance on the secondary side. Although the *LC* resonant network was proposed very early, yet unpopular recently, there are several justifications for adopting the *LC* resonant network.

1) The *LC* resonant network can overcome the shortcomings brought by the transformer. This article utilizes the *LC* resonant network and places it on the secondary side unusually to eliminate the weakness and take full advantage

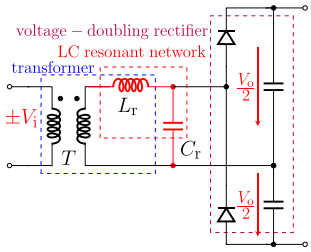

Fig. 5. Proposed step-up scheme of the converter.

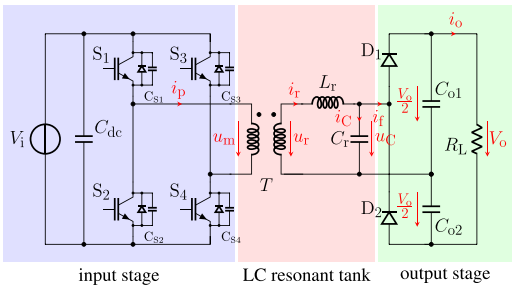

Fig. 6. *LC* resonant converter.

of the parameters of the transformer as a typical step-up unit.

2) The *LC* resonant network decreases the number of high-voltage elements, reducing the cost and stress considerations.
3) Compared with some resonant networks, such as the *LLC* resonant network, the series inductance in the *LC* resonant network does not decrease the step-up ratio.

With the design mentality shown in Fig. 5, the *LC* resonant network is suitable for the step-up power conversion with a high-ratio transformer. Besides, the variable G and fixed n share the step-up requirement, making it well-suited for applications with a wide input range, such as wind power and PV. Then, the *LC* resonant converter should be further analyzed.

B. LC Resonant Converter

The circuit topology for the proposed resonant converter is shown in Fig. 6, taking the full-bridge structure as an example. The topology comprises a full-bridge switch circuit consisting of S_1-S_4 with the associated parasitic capacitances C_{S1}-C_{S4}, a transformer with the resonant network, rectifier diodes, and the output capacitors C_{o1} and C_{o2}. The resonant network comprises the resonant inductance L_r and capacitance C_r.

The converter should be able to output a high step-up ratio voltage. When the input voltage of the wind turbine and the load condition change, the output voltage should be maintained.

C. Operating Principles

Considering i_f, u_C, i_r, i_C, i_{d1}, and i_{d2} are the current that flows to the rectifier, the voltage of C_r, current of L_r, C_r, D_1, and D_2, respectively, the operating principles of the proposed converter can be analyzed. Assuming that the semiconductor

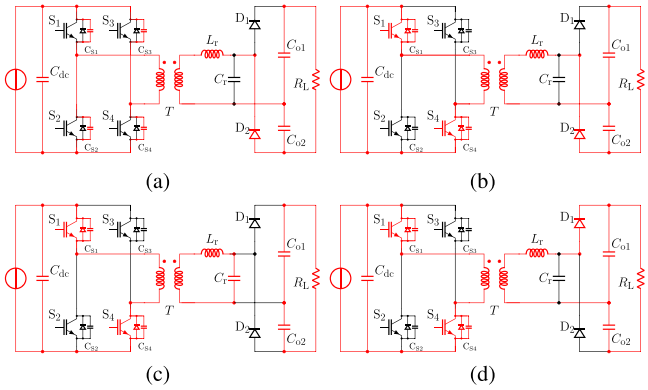

Fig. 7. Operating stages of the resonant converter. (a) Interval I. (b) Interval II. (c) Interval III. (d) Interval IV.

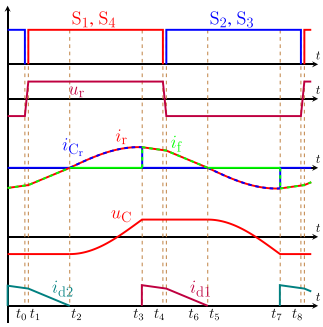

Fig. 8. Operating waveforms of the resonant converter.

switches and diodes are ideal components with a duty cycle of 0.5. The output capacitors are equal and large enough, and the voltages of which are equal and constant. The operating stages are revealed in Fig. 7, which has the following four intervals. The operating waveforms are shown in Fig. 8.

Interval I [t_0–t_1]: The parasitic capacitances of S_1 and S_2 are discharged and charged in the dead time, respectively.

Interval II [t_1–t_2]: S_1 turns ON with ZVS. C_r is clamped with D_2 conductive.

Interval III [t_2–t_3]: When i_f is zero, D_2 turns OFF with ZCS. C_r and L_r resonate. C_{o1} and C_{o2} provide power for the load.

Interval IV [t_3–t_4]: When u_C is $\frac{V_o}{2}$, D_1 is conductive, charging C_{o1}. The operating principles in the next half periods (t_4-t_8) are similar.

Neglecting the dead time, considering that $I_{r_{t1}}$ is the initial value of i_r at $t = t_1$, which is related to f_{sw} and can be calculated, if the resonant frequency is ω_r, the equations of the resonant process in three intervals can be calculated as

$$\begin{cases} i_r(t) = I_{r_{t1}} + (\frac{V_o}{2} + nV_i)(t - t_1) \\ u_C(t) = -\frac{V_o}{2} \end{cases} \tag{2}$$

$$\begin{cases} i_r(t) = \sqrt{\frac{C_r}{L_r}}(nV_i + \frac{V_o}{2})\sin(\omega_r(t - t_2)) \\ u_C(t) = nV_i - (nV_i + \frac{V_o}{2})\cos(\omega_r(t - t_2)) \end{cases} \tag{3}$$

$$\begin{cases} i_r(t) = 2\sqrt{\frac{C_r}{L_r}}\sqrt{nV_i\frac{V_o}{2}} + (nV_i - \frac{V_o}{2})(t - t_3) \\ u_C(t) = \frac{V_o}{2}. \end{cases} \tag{4}$$

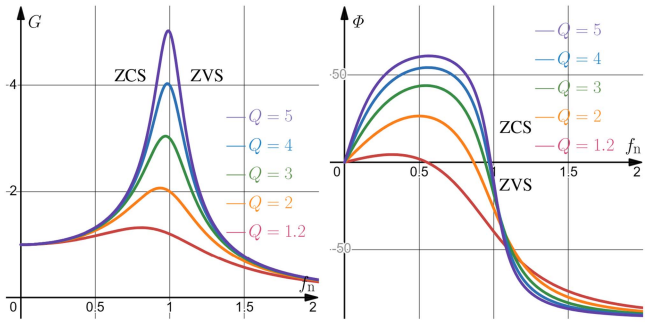

(a) (b)

Fig. 9. Output voltage gain and input current phase characteristics. (a) Gain curves. (b) Phase curves.

The initial value can also be found using the boundary conditions. These equations can confirm the voltage and current stress of the elements and help determine the value selection.

D. Resonant Characteristics

Although the resonant converter is not a new concept, the proposed converter extends its application, and more distinctive features appear. Using the fundamental harmonic model and considering that f_{r}, f_{n}, Z_{r}, R_{L}, R_{eq}, Q, Z_{i}, φ, and G represent the characteristic resonant frequency, normalized switching frequency, characteristic impedance, load resistance, ac equivalent resistance, quality factor, input resistance, power factor angle as well as the ZVS angle, and gain, respectively, the following equations can be derived:

$$\begin{cases} f_{\mathrm{r}} = \frac{\omega_{\mathrm{r}}}{2\pi} = \frac{1}{2\pi\sqrt{L_{\mathrm{r}}C_{\mathrm{r}}}} \\ f_{\mathrm{n}} = \frac{f_{\mathrm{sw}}}{f_{\mathrm{r}}} \\ Z_{\mathrm{r}} = \sqrt{\frac{L_{\mathrm{r}}}{C_{\mathrm{r}}}} \\ Q = \frac{R_{\mathrm{eq}}}{Z_{\mathrm{r}}} = \frac{2}{\pi^2}\sqrt{\frac{C_{\mathrm{r}}}{L_{\mathrm{r}}}}R_{\mathrm{L}} \\ Z_{\mathrm{i}} = \frac{j(Q^2 f_{\mathrm{n}}^3 + (1-Q^2)f_{\mathrm{n}}) + Q}{f_{\mathrm{n}}^2 Q^2 + 1} Z_{\mathrm{r}} \\ \varphi = -\arctan\frac{Q^2 f_{\mathrm{n}}^3 + (1-Q^2)f_{\mathrm{n}}}{Q} \\ G = \frac{V_{\mathrm{o}}}{2nV_{\mathrm{i}}} = \frac{1}{\sqrt{(1-f_{\mathrm{n}}^2)^2 + (\frac{f_{\mathrm{n}}}{Q})^2}}. \end{cases} \tag{5}$$

The output voltage gain and input current phase curves are plotted in Fig. 9 to analyze the resonant characteristics. Although uncommonly used, operating near f_{r} is more advantageous to meet the requirements of the step-up operating condition since the gain is high and varies more when adjusting the switching frequency f_{sw}.

The maximum gain is

$$G_{\max} = \sqrt{\frac{4Q^2}{4Q^2-1}}Q \gtrapprox G|_{f_{\mathrm{sw}}=f_{\mathrm{r}}} = Q \tag{6}$$

which suited the conditions well with a wide operating range. Thus, whether the converter can meet the step-up condition depends on the load condition. The converter is powerless if the load is too heavy, with a smaller Q, and $2nQ$ is less than the desired step-up ratio.

The frequency f_{r} is the most significant, however, an uncommonly used operating point. Hence, some characteristics are universally ignored. The step-up ability of the resonant network should be explored further, and the soft-switching issue needs more focus because the operating region is much nearer the ZCS region. In fact, $G_{\max}$ does not occur when $f_{\mathrm{n}} = 1$ because the current on the load branch impacts the resonance, causing the resonance point to shift. The angular frequency corresponding to the resonant point, ω_{r}, the maximum gain, ω_{Gmax}, and the pure resistive point, ω_{R}, are not the same, as

$$\begin{cases} \omega_{\mathrm{r}} = \frac{1}{\sqrt{L_{\mathrm{r}}C_{\mathrm{r}}}} \\ \omega_{\mathrm{Gmax}} = \sqrt{\frac{2Q^2-1}{2Q^2}}\omega_{\mathrm{r}} \\ \omega_{\mathrm{R}} = \sqrt{\frac{Q^2-1}{Q^2}}\omega_{\mathrm{r}}. \end{cases} \tag{7}$$

$G_{\max}$ is higher than but is approximately equal to Q. For example, $G_{\max} = 1.07Q$ when $Q = 1.4$. It can be regarded that $G_{\max} \approx Q$ when calculating the resonance parameter. When $\omega = \omega_{\mathrm{R}}$, $G = Q$. It can be observed that $\omega_{\mathrm{R}} < \omega_{\mathrm{Gmax}} < \omega_{\mathrm{r}}$ and f_{sw} should be limited above ω_{Gmax} as V_{o} can be regulated as it decreases monotonously as f_{sw} increases, and ZVS is guaranteed naturally. This is a beneficial characteristic. When Q is larger with a lighter load, it is easier to achieve ZVS. Although ω_{R} is smaller, f_{sw} is much higher to maintain the gain, as observed in the gain curves. When the load gets heavier, ω_{R} moves left, leaving more room for ZVS.

The *LC* resonant network may perform better than the *LLC* resonant network. With the same analysis method, it can be derived that the maximum gain of the *LLC* resonant network with the same Q value is not higher than the *LC* resonant network, especially the much larger leakage inductance, which serves as a series element that greatly decreases the gain. In addition, it can be deduced that $\omega_{\mathrm{R}} > \omega_{\mathrm{Gmax}} > \omega_{\mathrm{r}}$ in the *LLC* resonant network. Therefore, ZVS is much harder to ensure when pursuing a high gain.

The characteristic with the commonly used phase-shift control is also considered, and the gain can be derived as

$$G = \frac{1-\cos\delta}{2}\frac{1}{\sqrt{(1-f_{\mathrm{n}}^2)^2 + (\frac{f_{\mathrm{n}}}{Q})^2}} \tag{8}$$

where the phase-shift angle $\delta \in [0, \pi]$, and the gain characteristics are given in Fig. 10.

There are several reasons that the gain with phase-shift control should be analyzed. With phase-shift control, ZVS can be ensured forcibly by controlling the switches ON and OFF around the zero-crossing point of i_{r}. An *LC* resonant converter with phase-shift control could present a higher efficiency, which will be discussed later. Phase-shift control provides a new dimension of control, which handles the condition that the switching frequency is inconvenient to regulate higher. If the operating frequency is f_{r}, with phase-shift control, the phase-shift angle can be adjusted as

$$\Delta\delta = \pi - \arccos$$

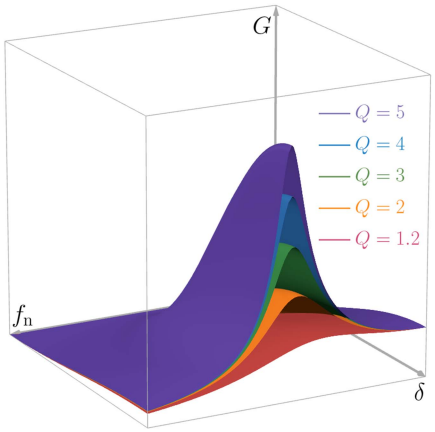

Fig. 10. Gain characteristics related to switching frequency and phase-shift angle.

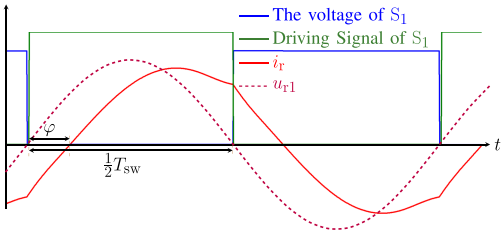

Fig. 11. Waveforms related to the soft-switching.

$$\left(1-\frac{2}{\sqrt{Q^2(1-(f_r+\Delta f_r))^2+(f_r+\Delta f_r)^2}}\right) \tag{9}$$

to get the same gain with the variable frequency (VF) control if Δf_r is regulated relatively slightly. Therefore, phase-shift control may avoid a sharp frequency regulation.

E. ZVS Analysis

One of the advantages of the resonant converter is that soft-switching reduces the power loss. The converter should operate in the inductive operating area. When the converter operates with a lighter load, f_{sw} should be higher, which makes it easy to achieve ZVS as illustrated above.

The fundamental waves of i_r and u_r transfer the active power, with the related waveforms shown in Fig. 11, considering that the fundamental value of u_r and i_r can be approximated as

$$\begin{cases} u_{r1}(t) = \frac{4n}{\pi} V_i \sin(2\pi f_{sw} t) \\ i_{r1}(t) = I_{rm} \sin(2\pi f_{sw} t - \varphi) \end{cases} \tag{10}$$

where I_{rm} is the peak value of i_r, it can be derived that

$$I_{rm} \cos\varphi = \frac{\pi V_o^2}{2nR_L V_i}. \tag{11}$$

Particularly, when operating at the maximum gain, $\varphi \approx 0$. The following equation can be derived:

$$I_{rm}|_{\varphi=0} = \frac{2V_o}{\pi Z_r}. \tag{12}$$

The current i_r seems to have a characteristic of constant current partially. Regardless of the load, the maximum voltage of C_r is $\frac{V_o}{2}$. The most amplitude of the resonant current is used to charge and discharge C_r, and the output current I_o is relatively small. Thus, i_r varies not much as the load changes. I_{rm} is smaller at a lighter load, while φ is larger.

Another ZVS condition is that the parasitic capacitances C_{oes} of the switches should be charged and discharged completely by the resonant current during the dead time, as

$$T_{dead} > \frac{V_i C_{oes}}{nI_{rm}\sin\varphi} = \frac{V_i C_{oes}}{nI_{rm}\sin(\arccos\frac{\pi V_o^2}{2nR_L V_i I_{rm}})}. \tag{13}$$

To estimate the hardest condition for ZVS, I_{rm} can be expressed as

$$I_{rm} = \frac{2V_o\sqrt{(Q^2 f_n^3 + (1-Q^2)f_n)^2 + Q^2}}{\pi Z_r Q\sqrt{Q^2(1-f_n^2)^2 + f_n^2}}. \tag{14}$$

The right side of the equation is monotonous, and T_{dead} should be larger as the load is lighter within the reasonable operating range. Especially, achieving ZVS is particularly difficult at no load condition, when the minimum T_{dead} should satisfy that

$$T_{dead}|_{R_L=\infty} > \frac{\pi C_{oes} Z_r |f_n^2 - 1|}{4n^2 f_n}. \tag{15}$$

The converter steps up the voltage by the resonant network, which operates much closer to the ZCS region. Once the converter crosses the boundary and operates at the ZCS region, the gain decreases as f_{sw} decreases, bringing the disorder to the control. Therefore, the switching frequency f_{sw} should be kept within a reasonable range in the control method.

F. Power Loss

The power loss of the whole circuit mainly includes the switching loss P_{sw}^{loss}, the transformer loss P_T^{loss}, and the rectifier loss P_{rec}^{loss}, with the transformer loss being the majority.

The power loss of the transformer mainly includes copper loss and iron loss. The power loss of semiconductor switches and the rectifier loss are mainly the conducting loss due to soft switching. They can be expressed approximately as

$$\begin{cases} P_T^{loss} \approx \frac{1}{2} I_{rm}^2 R_T + p_T f_{sw}^{\alpha} \\ P_{sw}^{loss} \approx \frac{2}{\pi}\int_{\varphi}^{\pi} nV_{con} I_{rm} \sin(\omega_{sw} t - \varphi) \mathrm{d}(\omega_{sw} t) = \frac{2V_{con}V_o^2}{R_L V_i} \\ P_{rec}^{loss} \approx V_{rec} I_o \end{cases} \tag{16}$$

where ω_{sw}, R_T, and p_T are the switching angular frequency, the equivalent series resistance of the transformer, and a constant related to the iron-core material, operating condition, design parameters, etc. α is an empirical parameter that generally takes a value of 1.7-2. V_{con} and V_{rec} represent the saturation voltage drop of the primary switches and the forward conduction voltage of the rectifier diodes. The efficiency can be increased mainly by improving the design of the high-frequency transformer, which will be discussed later.

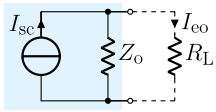

Fig. 12. Open-loop steady-state output equivalent circuit of the resonant converter.

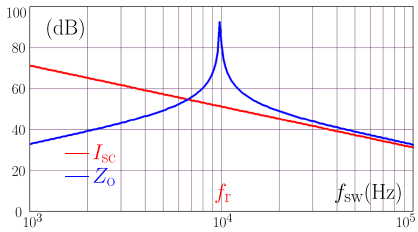

(a)

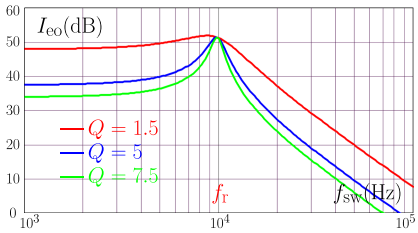

(b)

Fig. 13. Amplitude-frequency characteristic of I_{sc}, Z_o, and I_{eo}. (a) Amplitude-frequency characteristic of I_{sc} and Z_o. (b) Amplitude-frequency characteristic of I_{eo}.

G. External Characteristics

There are different methods to control a dc/dc converter in the dc power system, such as main–secondary control, voltage margin control, and voltage droop control. Traditional open-loop dc/dc converters generally have the characteristics of a voltage source, but the proposed dc/dc converter with the resonant network has a different output characteristic. In ideal conditions, the steady-state open-loop output equivalent circuit on the ac side of the high-voltage rectifier can be simplified into the current source model, as shown in Fig. 12. Considering that Z_o, I_{sc}, and I_{eo} indicate the output equivalent impedance, output short-circuit current, and equivalent output current, respectively, whose amplitude-frequency characteristics are shown in Fig. 13. They can be derived as

$$\begin{cases} Z_o(s) = \frac{sL_r}{s^2L_rC_r+1} \\ I_{sc}(s) = \frac{nV_i}{sL_r} \\ I_{eo}(s) = \frac{nV_i}{sL_r+\frac{2R_L}{\pi^2}(s^2L_rC_r+1)}. \end{cases} \tag{17}$$

Especially, $|Z_o(j\omega_r)| = \infty$, and $|I_{sc}(j\omega_r)| = |I_{eo}(j\omega_r)| = \frac{nV_i}{Z_r}$. The maximum output current is independent of the load at f_r, presenting the characteristics of the constant current source, completely different from the output voltage source characteristics of the traditional converters. Thus, the converter has a strong ability to handle external dc bus short-circuit faults. Further investigation into the grid-connected control of the resonant converter may be worthwhile.

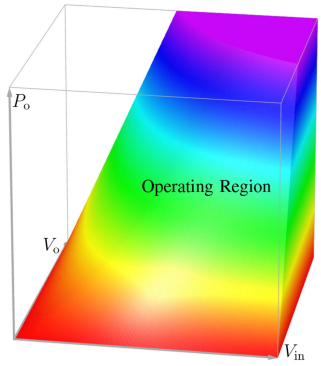

Fig. 14. Voltage and power characteristics.

The gain is approximately inversely proportional to the output power P_o, as

$$P_oQ = \frac{2}{\pi^2}\sqrt{\frac{C_r}{L_r}}V_o^2. \tag{18}$$

When the input power decreases, the gain will rise automatically to maintain V_o with a higher Q. The maximum output power boundary can be calculated as

$$P_{o,max}(t) = \frac{2}{\pi^2}\sqrt{\frac{C_r}{L_r}}V_oV_i(t). \tag{19}$$

The voltage and power characteristics can be presented in Fig. 14. If V_o is maintained, the relationship between P_o and V_i is approximately linear, suitable for wind or PV power. The converter can cooperate well with the wind turbines, and the generator may be connected only by a rectifier without the boost PWM converter if controlled well.

The step-up ratio and transmission power of the resonant network are closely linked to Q, Z_r, and f_r. Therefore, by selecting appropriate resonance parameters, it is possible to meet the requirements of the step-up ratio and power.

H. Discussion of the Filter Inductor

The *LC* resonant converter is a classical but less-used resonant converter. To smooth the secondary current, an inductor L_f is usually attached to form an *LC* filter with the output capacitor in practical applications, consisting of an *LCL-T* resonant network. As a high step-up converter, the peak value of the secondary current is relatively high because of the discontinuity, however, the impact of L_f needs more investigation. Considering that k_L, f_{r1}, f_{r2}, ω_{r1}, and ω_{r2} represent the ratio of the L_f to L_r, characteristic resonant frequencies, and angular frequencies, the

following equations can be derived:

$$\begin{cases} k_{\mathrm{L}} = \frac{L_{\mathrm{f}}}{L_{\mathrm{r}}} \\ f_{\mathrm{r1}} = \frac{\omega_{\mathrm{r1}}}{2\pi} = \frac{1}{2\pi\sqrt{L_{\mathrm{r}}C_{\mathrm{r}}}} \\ f_{\mathrm{r2}} = \frac{\omega_{\mathrm{r2}}}{2\pi} = \frac{1}{2\pi\sqrt{(L_{\mathrm{r}}//L_{\mathrm{f}})C_{\mathrm{r}}}} = \frac{1}{2\pi\sqrt{\frac{k_{\mathrm{L}}}{k_{\mathrm{L}}+1}L_{\mathrm{r}}C_{\mathrm{r}}}} \\ Z_{\mathrm{i}} = \frac{j(k_{\mathrm{L}}^2 f_{\mathrm{n}}^5+(Q^2-k_{\mathrm{L}}^2-2k_{\mathrm{L}})f_{\mathrm{n}}^3+(-Q^2+k_{\mathrm{L}}+1)f_{\mathrm{n}})+Q}{k_{\mathrm{L}}^2 f_{\mathrm{n}}^4-2f_{\mathrm{n}}^2 k_{\mathrm{L}}+f_{\mathrm{n}}^2 Q^2+1} Z_{\mathrm{r}} \\ \varphi = -\arctan\frac{k_{\mathrm{L}}^2 f_{\mathrm{n}}^5+(Q^2-k_{\mathrm{L}}^2-2k_{\mathrm{L}})f_{\mathrm{n}}^3+(-Q^2+k_{\mathrm{L}}+1)f_{\mathrm{n}}}{Q} \\ G = \frac{V_{\mathrm{o}}}{2nV_{\mathrm{i}}} = \frac{1}{\sqrt{(1-f_{\mathrm{n}}^2)^2+(\frac{f_{\mathrm{n}}}{Q}(1+k_{\mathrm{L}}-k_{\mathrm{L}}f_{\mathrm{n}}^2))^2}}. \end{cases} \tag{20}$$

Using the same method mentioned above, it can be derived that

$$\begin{cases} \omega_{\mathrm{r1}} = \frac{1}{\sqrt{L_{\mathrm{r}}C_{\mathrm{r}}}} \\ \omega_{\mathrm{Gmax}} = \sqrt{\frac{2k_{\mathrm{L}}+2k_{\mathrm{L}}^2-Q^2+\sqrt{k_{\mathrm{L}}^4+2k_{\mathrm{L}}^3+k_{\mathrm{L}}^2+2k_{\mathrm{L}}^2Q^2-4k_{\mathrm{L}}Q^2+Q^4}}{3k_{\mathrm{L}}^2L_{\mathrm{r}}C_{\mathrm{r}}}} \\ \omega_{\mathrm{R}} = \sqrt{\frac{k_{\mathrm{L}}^2+2k_{\mathrm{L}}-Q^2+\sqrt{Q^4+2k_{\mathrm{L}}^2Q^2-4k_{\mathrm{L}}Q^2+k_{\mathrm{L}}^4}}{2k_{\mathrm{L}}^2L_{\mathrm{r}}C_{\mathrm{r}}}} \end{cases} \tag{21}$$

and

$$G_{\max} \gtrapprox Q. \tag{22}$$

The conclusion $\omega_{\mathrm{R}} < \omega_{\mathrm{Gmax}} < \omega_{\mathrm{r1}}$ remains. Using the gain curves, it can be observed that the gain varies not greatly as k_{L} varies from 0 to 1. In addition, it changes little in the range that $0.5 < k_{\mathrm{L}} < 1$, and it can be regarded that $G_{\max}$ occurs at $f_{\mathrm{n}} = 1$. Therefore, it can be seen that though L_{f} is commonly used in practice, the *LC* resonant network and *LCL-T* resonant network do not show many essential differences from the view of the gain, and L_{f} does not greatly affect the step-up performance. The differences between the *LC* resonant network and the *LCL-T* resonant network are more in the operating conditions.

By plotting the amplitude-frequency characteristics of the *LCL-T* resonant network, it can be seen that the *LCL-T* and *LC* resonant networks both behave as a current source at the output. However, at the other characteristic resonant frequency f_{r2}, the short-circuit current is very large. Therefore, it is better to avoid operating around f_{r2}.

Fig. 15 shows the resonant current and voltage, and the oscillation of the current of the secondary diodes D_1 and D_2 is large in the *LC* parallel resonant converter. However, it cancels a resonant inductor and related power loss and still realizes turn-OFF with ZCS. L_{f} functions as a filter, especially with a larger Q.

Several factors may be affected by L_{f} as follows:

1) L_{f} prolongs the conducting time of i_{f} while it does not change the average value, and smooths i_{f}, though the peak value of i_{f} is not necessarily smaller. L_{f} makes the diodes achieve ZCS turn-ON and avoid the oscillation distinctly, reducing the current stress of the diodes.
2) L_{f} increases the amplitude of u_{C} by resonance, and the withstand voltage of C_{r} is not $\frac{V_{\mathrm{o}}}{2}$ anymore, which is unfavorable for high-voltage applications.
3) L_{f} may reduce i_{r} and the output ripples very slightly.
4) L_{f} adds the number of components, unbeneficial to the efficiency and cost.

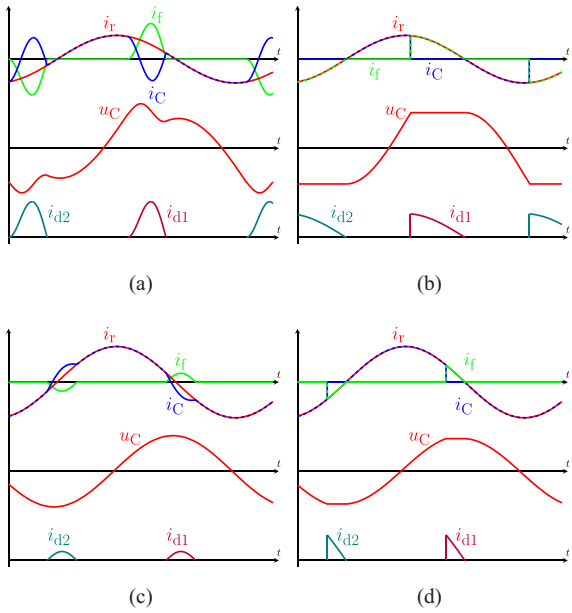

Fig. 15. Resonant current and voltage of different resonant networks and Q. (a) *LCL-T* resonant network with a smaller Q. (b) *LC* parallel resonant network with a smaller Q. (c) *LCL-T* resonant network with a larger Q. (d) *LC* parallel resonant network with a larger Q.

5) The undesired high-frequency resonance appears with a small L_{f}, especially with a large L_{r}.

Besides, when L_{f} is large enough, the enhancement of the filter effect is obviously weakened as L_{f} gets larger, and the disadvantages of L_{f} become more significant. However, considering that the high-voltage components should be saved as much as possible, and the advantageous effect of L_{f} is relatively limited, it may not be better to utilize L_{f} in this situation.

Another scheme is putting the *LCL-T* resonant network on the primary side by using the leakage inductance as L_{f} with resonant inductance L_{r}' and capacitance C_{r}' added. This structure reduces some disadvantages above, and lowers the voltage stress of the capacitance. However, it increases the current stress of the capacitance, as well as its value and size, and the voltage of the transformer is increased, making it easier to reach saturation. Besides, it reduces the utilization rate of the transformer with another inductance on the primary side needed, which also increases the component number and loss. Therefore, this scheme may not perform better than that if the *LC* resonant network is on the secondary side under the step-up application scenario with a high-ratio transformer, though generally the *LCL-T* network may be preferred over the *LC* resonant network in other applications.

III. Transformer Design and Optimization

A. Transformer Design

As mentioned, the separated winding is utilized for insulation considerations. The large leakage inductance is decided by n while determining Q, which are the two determinants of the step-up ratio. Thus, the optimization revolves around L_{r} is a significant problem, and the conventional design method combined with the resonant network is not suitable.

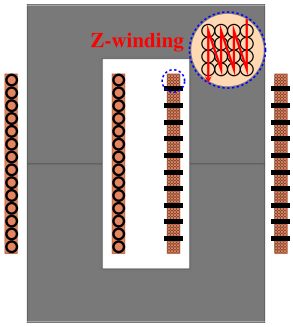

Fig. 16. Section diagram of the transformer with separated winding.

The transformer with a separated winding can utilize the UU-type frame with Z-type winding in multiple slots to share the high voltage and enhance the insulating ability, as shown in Fig. 16. The dimension of the core and winding is calculated with parameters such as the layer number of winding, wire specification, and insulation distance determined, which lays the foundation of the design. Sequentially, many parameters are decided, such as the iron loss coefficients K, α, β, and ac resistance coefficients and dc resistances of the primary and secondary side, F_{rp}, F_{rs}, and R_{dcp}, R_{dcs}. Then, the key parameter L_{r} can be determined using the method in [24].

B. Optimization Between Transformer Ratio and Resonant Gain

The good cooperation between the transformer and resonant network helps to improve the step-up ratio and reduce the power loss. When the resonant network operates at the maximum gain, it has the maximum step-up ratio $2nQ$. The resonant network, especially the elements L_{r} and C_{r}, is used and operates around f_{r} to raise the voltage, which is uncommon in other resonant converters. The resonant network should not operate with an extremely high Q to achieve a very high gain, as it causes a large reactive current and more power loss. However, a small Q means a large n and a large number of turns, influencing the operation and bringing difficulties for the design since L_{r} is proportional to the square of the turns. Thus, it is necessary to select balanced Q and n based on the step-up ratio with efficiency considered.

As is well-known, the turns ratio is $n = \frac{N_2}{N_1}$, and the leakage inductance $L_{\mathrm{r}} = N_2^2 \Lambda$ is determined by the leakage permeance Λ and ratio, where Λ is related to the dimension and structure of the transformer. For another, in the *LC* resonant converter, L_{r} is the key component of the resonant network, determining the quality factor and gain, as

$$L_{\mathrm{r}} = \frac{2V_{\mathrm{o}}^2}{\pi^2 P_{\mathrm{o}} \omega_{\mathrm{r}} Q}. \tag{23}$$

Considering the total step-up ratio is $2nQ$, it can be derived that to meet the requirement of the step-up ratio, the following equation should be satisfied:

$$N_1 N_2 \le \frac{2V_{\mathrm{o}}^2}{\pi^3 k_{\mathrm{boost}} P_{\mathrm{o}} f_{\mathrm{sw}} \Lambda}. \tag{24}$$

Thus, the desired leakage inductance L_{r} can be obtained in theory with the production of N_1 and N_2 less than a constant.

The magnitude of the magnetic induction intensity B_{m} is

$$B_{\mathrm{m}} = \frac{u_{\mathrm{m}}}{K_{\mathrm{c}} K_{\mathrm{f}} f_{\mathrm{sw}} N_1 A_{\mathrm{c}}} \tag{25}$$

where the magnetizing voltage u_{m} is a square wave whose amplitude approximately equals nV_{i}, K_{f} is the waveform factor that equals 4 approximately for the square wave, K_{c} is the lamination factor, and A_{c} is the sectional area of the iron core. B_{m} should be considered for both efficiency calculation and saturation check, where the maximum magnetic induction intensity appears in the middle of the secondary winding due to the leakage flux.

The loss is calculated by the improved generalized Steinmetz equation and the Dowell equation, as

$$P_{\mathrm{loss}} = V_{\mathrm{c}} K 2^{\alpha+\beta} f_{\mathrm{sw}}^{\alpha} B_{\mathrm{m}}^{\beta} + F_{\mathrm{rp}} I_{\mathrm{p}}^2 R_{\mathrm{dcp}} + F_{\mathrm{rs}} I_{\mathrm{r}}^2 R_{\mathrm{dcs}} \tag{26}$$

where V_{c} is the volume of the transformer. Since the dimension and structure are fixed, N_1 can be substituted into the equation, and by taking the derivative of N_1, there is an optimal value of N_1 to make the loss minimum

$$N_1 \approx \frac{V_{\mathrm{i}}}{K_{\mathrm{c}} K_{\mathrm{f}} A_{\mathrm{c}}} \sqrt[\beta]{\frac{2^{\alpha+\beta} \beta K V_{\mathrm{c}} f_{\mathrm{sw}}^{\alpha-\beta}}{F_{\mathrm{rp}} I_{\mathrm{p}}^2 R_{\mathrm{dcp}} + F_{\mathrm{rs}} I_{\mathrm{r}}^2 R_{\mathrm{dcs}}}}. \tag{27}$$

Then, N_2 and the value of inductance can be easily obtained. The magnetizing inductance of the transformer L_{m} hardly affects the resonant process and the step-up capacity because it is in parallel with the resonant network and directly connected to the input equivalently. It should be as small as possible to improve efficiency. Based on this method, though there is a coupling of Q and n with L_{r} linked, the step-up ratio is satisfied with power loss minimized.

It should be noted that considering the volume of the transformer is partly decided by the windings, which is also related to L_{r}. Therefore, the L_{r} also decides the power density of the transformer. With actual computation, it can be derived that the efficiency and power density are contradictory. Therefore, the compromise design should be carried out to solve this problem with other tools, such as a Pareto diagram.

Generally, the specific design process of a high-voltage high-frequency transformer is relatively complex with a large number of variables and many equations, which can be summarized as Fig. 17.

C. Design Example

Limited by the conditions of the test instruments, the output voltage and power are 3 kV and 3 kW, respectively, and the minimum step-up ratio is 65. To be simple but general, this article takes the manganese zinc ferrite with Litz wire transformer in the prototype as an example to verify the feasibility, though amorphous alloy core and flat-type copper wire may perform better for a megawatt-level transformer to improve efficiency, space utility, and current carrying capacity. The parameters of the wire are calculated using the value of current and the skin effect depth. Based on the optimization design procedure when focusing more on the efficiency, the transformer can be designed,

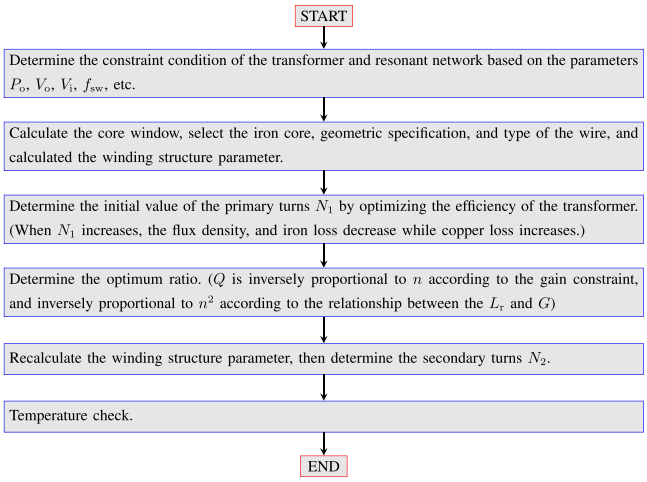

Fig. 17. Optimization design of Q and n.

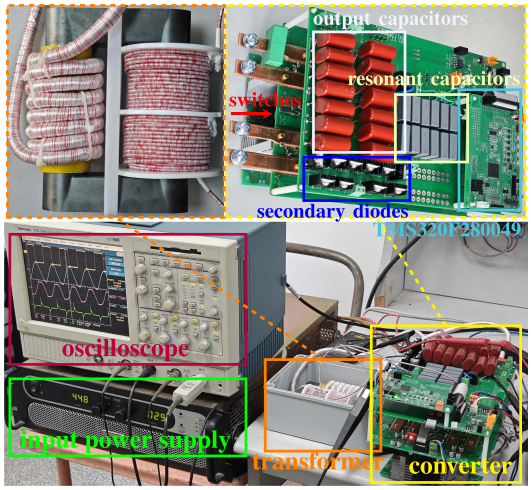

Fig. 18. Experimental prototype figure with transformer and main converter enlarged.

TABLE I
TRANSFORMER SPECIFICATIONS

Parameters	Values/types
Magnetic core	UY30
Turns ratio $N_1 : N_2$	7:160
Layers of primary/secondary side	1 / 4
Length of each turn for primary/secondary side[m]	0.13 / 0.135
Leakage inductance [mH]	7
Magnetizing inductance [mH]	167

with the specifications shown in Table I, where N_2 takes the maximum value in the design to reduce Q and reactive power loss. The leakage inductance and magnetizing inductance are obtained, both equivalent to the secondary side.

Based on the step-up ratio, output voltage, and power, Q can be selected as 1.4, and $Z_r = 434.2\,\Omega$ with C_r calculated as 37.1 nF according to the resonant relationship. Although Q is not very large, it achieves an optimum allocation between Q and n from the perspective of efficiency based on the optimization design method. In addition, Q should have a large range to handle different operating conditions, which will become larger with a lighter load. Besides, though the power density is lower compared with the compact structure, it is unavoidable considering the insulation. The large turns and layers in the secondary side may not greatly affect the power density because of the small secondary current, and the volume can be further optimized if necessary.

IV. EXPERIMENTAL VERIFICATION

The experimental set-up shown in Fig. 18 is built to verify the validity of the proposed resonant converter. Table II shows the design specifications of the prototype based on the optimization design. VF control and variable frequency phase-shift (VFPS) control are utilized. The ZVS angle is fixed at a small value in the VFPS control, with the phase-shift angle regulating the output voltage, hence, the ZVS feature will not be lost. Because of the large value of the input current, the ripples should be considered. However, the input current depends on I_{rm}, which is determined by the operating condition. Thus, the ripples are not easy to reduce through control, and adding the input inductor causes the voltage stress of the switches to be uncertain. Thus, the simple and easy method is to attach input capacitors. Fortunately, the size and cost are small with a low input voltage.

TABLE II
CIRCUIT SPECIFICATIONS IN THE PROTOTYPE

Parameters	Values/components
Rated Input Voltage V_i[V]	46
Output Voltage V_o[V]	3000
Minimum Step-up Ratio	65
Rated Output Power P_o[W]	3000
Leakage inductance L_r[mH]	7
Resonant Capacitor C_r[nF]	37.5
Output Capacitors C_{o1}, C_{o2}[μF]	7
Semiconductor Switches S_1-S_4	IRFB4310
Rectifier Diodes D_1, D_2	VS-20ETF12
DSP Controller	TMS320F280049
Switching frequency f_{sw}[kHz]	10–16
Input filter capacitors [μF]	30×2200

Fig. 19(a) presents the measured input voltage V_i, two output voltages $+\frac{V_o}{2}$ and $-\frac{V_o}{2}$, resonant current i_r, and calculated output voltage V_o at the full load condition of 3 kW with VF control. V_o can be maintained at approximately 3000 V steadily as desired with a step-up ratio of 65. Fig. 19(b) presents the measured primary input voltage u_m, primary input current i_p, resonant capacitor voltage u_C, and resonant inductor current i_f at full load condition with VF control. ZVS of the switches and ZCS of the diodes are realized. Fig. 19(c) and (d) presents the waveforms with VFPS control, and the converter obtains good results as that with VF control.

The waveforms at the load condition of 500 W shown in Fig. 20 demonstrate the wide operating range of the converter. The measured input voltage and output voltage are the same as those in Fig. 19(a) and (b).

The maximum step-up ratio is about $2nQ$, where n is fixed. The actual voltage regulation method to handle the varying operating conditions is regulating Q. When operating with low

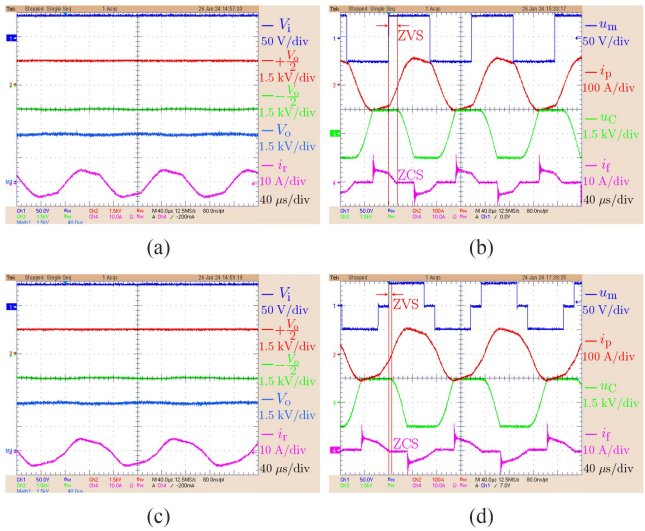

Fig. 19. Experimental results with a full load of 3 kW. (a) Measured V_{i}, $+\frac{V_{\mathrm{o}}}{2}$, $-\frac{V_{\mathrm{o}}}{2}$, i_{r}, and calculated V_{o} with VF control. (b) Measured u_{m}, i_{p}, u_{C}, and i_{f} with VF control. (c) Measured V_{i}, $+\frac{V_{\mathrm{o}}}{2}$, $-\frac{V_{\mathrm{o}}}{2}$, i_{r}, and calculated V_{o} with VFPS control. (d) Measured u_{m}, i_{p}, u_{C}, and i_{f} with VFPS control.

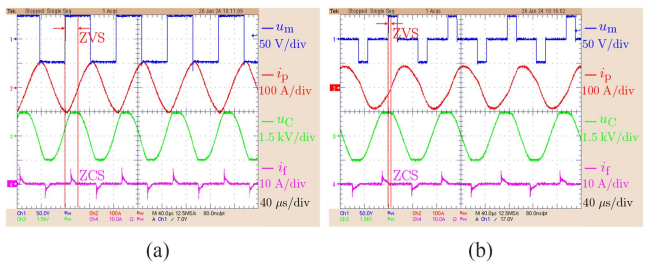

Fig. 20. Experimental results with a load of 500 W. (a) Measured u_{m}, i_{p}, u_{C}, and i_{f} with VF control. (b) Measured u_{m}, i_{p}, u_{C}, and i_{f} with VFPS control.

input, the converter should be able to elevate the output by raising Q. The experiment, whose input and output are 10.8 V and 3000 V, respectively, is carried out with a load of 500 W. On this occasion, the Q value is 6, which is higher than before, and the step-up ratio is 278. The experimental results are shown in Fig. 21, verifying the strong step-up ability under severe operating conditions.

The efficiency curves are plotted in Fig. 22(a). The efficiency reaches 97.4% and 90.4% at 3000 W and 500 W with the input voltage of 46 V. When V_{i} is 10.8 V, and P_{o} is 500 W, the efficiency reaches 92.8% . The efficiency of VFPS control is generally higher than VF control with the same voltage and power, and the efficiency with a lower input voltage is higher than that with a higher input because the reactive power reduces as the input voltage gets lower, according to the current source characteristic of the resonant tank. The converter may perform more efficiently than many conventional multiple dc-dc converters with the same step-up ratio. Fig. 22(b) provides the loss distribution, in which the transformer loss predominates.

There are a few high step-up resonant converters with different types, containing single-stage structure converters (such as

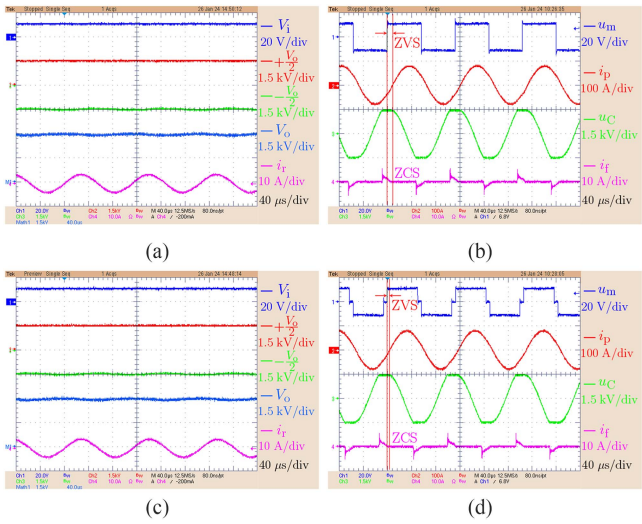

Fig. 21. Experimental results under an input voltage of 10.8 V with a load of 500 W. (a) Measured V_{i}, $+\frac{V_{\mathrm{o}}}{2}$, $-\frac{V_{\mathrm{o}}}{2}$, i_{r}, and calculated V_{o} with VF control. (b) Measured u_{m}, i_{p}, u_{C}, and i_{f} with VF control. (c) Measured V_{i}, $+\frac{V_{\mathrm{o}}}{2}$, $-\frac{V_{\mathrm{o}}}{2}$, i_{r}, and calculated V_{o} with VFPS control. (d) Measured u_{m}, i_{p}, u_{C}, and i_{f} with VFPS control.

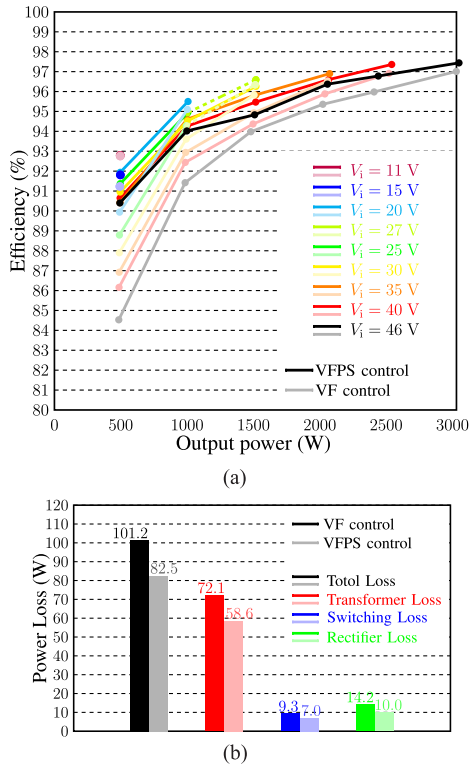

Fig. 22. Efficiency of the converter. (a) Efficiency curves. (b) Loss distribution.

in [15] and [16]) and converters with modules (such as in [19] and [23]), and many other structures. A comparison of some different existing high step-up resonant converters is given in Table III. The proposed converter shows high efficiency and a small number of components, and the stress voltage of the

TABLE III
COMPARISON OF DIFFERENT HIGH STEP-UP RESONANT CONVERTERS

Converters		in [12]	in [13]	in [15]	in [16]	in [17]	in [19]	in [20]	in [21]	in [23]	Proposed
Number of	Switches	4	2	4	2	4	5	7	6	4	4
	Diodes	10	6	2	3	0	9	3	2	8	2
	Inductors	4	0	2	1	0	4	1	1	1	0
	Capacitors	7	6	5	5	4	5	4	3	11	4
	Transformers	0	1	1	1	1	0	1	2	1	1
Input voltage [V]		120–320	30	20–30	20	40–50	75	30–60	150	500	10.8–46
Output voltage [V]		1000	380	400	400	380	1800	200–400	1500	2700	3000
Step-up ratio		3.1–8.3	12.7	13.3–20	20	7.6–9.5	24	3.3–13.3	10	5.4	65–278
Output power [W]		1300	200	2000	250	400	2000	500	2000	3700	3000
Switch voltage stress [V]		–	$0.2V_{\mathrm{o}}$	–	$2.7V_{\mathrm{i}}$	–	$8V_{\mathrm{i}}$	V_{i}	V_{i}	$0.5V_{\mathrm{i}}$	V_{i}
Maximum efficiency [%]		96.5	96.3	95.5	96.7	97.0	–	95.4	97.1	98.8	97.4

switches is acceptable. Moreover, a very high step-up ratio is realized, which is tenfold larger than that of some existing step-up resonant converters, proving the advantages of the converter.

V. CONCLUSION

A high step-up dc/dc resonant converter that can be used for high-voltage dc collection in the dc wind farm is proposed in the article. Through analysis and experimental verification, the following conclusions are obtained.

1) The proposed resonant converter overcomes and makes full use of the disadvantages of the large ratio high-voltage transformer with primary and secondary winding separation, realizing the integration of transformer and resonant network and making the converter efficient.
2) The converter achieves a very high step-up ratio by the multistage step-up units in a single resonant structure.
3) Through the optimized design between the transformer ratio and the resonance gain, the step-up ratio reaches hundreds of times, which can meet the demand of the single-stage step-up network configuration.
4) The power and step-up ratio characteristic is very suitable for the output power-voltage characteristic of the wind turbines. Besides, the proposed converter has the output characteristics of the current source and can cope with faults such as the short circuit of the output dc bus with ease.
5) The efficiency of the converter using VFPS control is higher than that of VF control, achieving 97.4% with soft-switching characteristics.

The experimental results align with the theoretical analysis and demonstrate the feasibility of the proposed converter. The step-up ratio is not only 65-278 in the experiment, but can also be increased depending on the practical need. Furthermore, the grid-connected control of the resonant converter requires further investigation.

REFERENCES

[1] N. Flourentzou, V. G. Agelidis, and G. D. Demetriades, "VSC-based HVDC power transmission systems: An overview," *IEEE Trans. Power Electron.*, vol. 24, no. 3, pp. 592–602, Mar. 2009.

[2] D. Van Hertem, M. Ghandhari, and M. Delimar, "Technical limitations towards a supergrid—A European prospective," in *Proc. IEEE Int. Energy Conf.*, 2010, pp. 302–309.

[3] H. J. Bahirat, B. A. Mork, and H. K. Høidalen, "Comparison of wind farm topologies for offshore applications," in *Proc. IEEE Power Energy Soc. Gen. Meeting*, 2012, pp. 1–8.

[4] J. D. Paez, D. Frey, J. Maneiro, S. Bacha, and P. Dworakowski, "Overview of DC-DC converters dedicated to HVDC grids," *IEEE Trans. Power Del.*, vol. 34, no. 1, pp. 119–128, Feb. 2019.

[5] D. Jovcic, "Bidirectional, high-power DC transformer," *IEEE Trans. Power Del.*, vol. 24, no. 4, pp. 2276–2283, Oct. 2009.

[6] A. Parastar and J.-K. Seok, "High-gain resonant switched-capacitor cell-based DC/DC converter for offshore wind energy systems," *IEEE Trans. Power Electron.*, vol. 30, no. 2, pp. 644–656, Feb. 2015.

[7] Z. Ou, G. Wang, and L. Zhang, "Modular multilevel converter control strategy based on arm current control under unbalanced grid condition," *IEEE Trans. Power Electron.*, vol. 33, no. 5, pp. 3826–3836, May 2018.

[8] G. Ning et al., "A hybrid resonant ZVZCS three-level converter for MVDC-connected offshore wind power collection systems," *IEEE Trans. Power Electron.*, vol. 33, no. 8, pp. 6633–6645, Aug. 2018.

[9] C. Dincan, P. Kjaer, Y.-H. Chen, S. Munk-Nielsen, and C. L. Bak, "Analysis of a high-power, resonant DC-DC converter for DC wind turbines," *IEEE Trans. Power Electron.*, vol. 33, no. 9, pp. 7438–7454, Sep. 2018.

[10] R. Yin, M. Shi, W. Hu, J. Guo, P. Hu, and Y. Wang, "An accelerated model of modular isolated DC/DC converter used in offshore DC wind farm," *IEEE Trans. Power Electron.*, vol. 34, no. 4, pp. 3150–3163, Apr. 2019.

[11] H. Tarzamni, H. S. Gohari, M. Sabahi, and J. Kyyrä, "Nonisolated high step-up DC-DC converters: Comparative review and metrics applicability," *IEEE Trans. Power Electron.*, vol. 39, no. 1, pp. 582–625, Jan. 2024.

[12] R. Beiranvand and S. H. Sangani, "A family of interleaved high step-up DC-DC converters by integrating a voltage multiplier and an active clamp circuits," *IEEE Trans. Power Electron.*, vol. 37, no. 7, pp. 8001–8014, Jul. 2022.

[13] R. Fani, E. Farshidi, E. Adib, and A. Kosarian, "Analysis, design, and implementation of a ZVT high step-up DC-DC converter with continuous input current," *IEEE Trans. Ind. Electron.*, vol. 67, no. 12, pp. 10455–10463, Dec. 2020.

[14] X. Zhao, C.-W. Chen, J.-S. Lai, and O. Yu, "Circuit design considerations for reducing parasitic effects on GAN-based 1-MHz high-power-density high-step-up/down isolated resonant converters," *IEEE Trans. Emerg. Sel. Topics Power Electron.*, vol. 7, no. 2, pp. 695–705, Jun. 2019.

[15] F. Shang, G. Niu, and M. Krishnamurthy, "Design and analysis of a high-voltage-gain step-up resonant DC-DC converter for transportation applications," *IEEE Trans. Transport. Electrific.*, vol. 3, no. 1, pp. 157–167, Mar. 2017.

[16] K. Zaoskoufis and E. C. Tatakis, "Isolated ZVS-ZCS DC-DC high step-up converter with low-ripple input current," *IEEE J. Emerg. Sel. Topics Ind. Electron.*, vol. 2, no. 4, pp. 464–480, Oct. 2021.

[17] S. Son, O. A. Montes, A. Junyent-Ferré, and M. Kim, "High step-up resonant DC/DC converter with balanced capacitor voltage for distributed generation systems," *IEEE Trans. Power Electron.*, vol. 34, no. 5, pp. 4375–4387, May 2019.

[18] Y. Yue and G. Wang, "An LLC-based single-stage step-up AC/DC resonant converter without boost circuit for EV charging with high power factor," *IEEE Trans. Power Electron.*, vol. 39, no. 6, pp. 7156–7166, Jun. 2024.

[19] X. Zhu, L. Jiang, B. Zhang, and K. Jin, "The resonant modular multilevel dc-dc converter adopting switched-inductor cells for high step-up ratio," *IEEE Trans. Emerg. Sel. Topics Power Electron.*, vol. 10, no. 6, pp. 6634–6647, Dec. 2022.

[20] Y. Shen, H. Wang, A. Al-Durra, Z. Qin, and F. Blaabjerg, "A structure-reconfigurable series resonant DC-DC converter with wide-input and configurable-output voltages," *IEEE Trans. Ind. Appl.*, vol. 55, no. 2, pp. 1752–1764, Mar./Apr. 2019.
[21] L. Shu et al., "A resonant ZVZCS DC-DC converter with two uneven transformers for an MVDC collection system of offshore wind farms," *IEEE Trans. Ind. Electron.*, vol. 64, no. 10, pp. 7886–7895, Oct. 2017.
[22] M. Abbasi and J. Lam, "A modular SiC-based step-up converter with soft-switching-assisted networks and internally coupled high-voltage-gain modules for wind energy system with a medium-voltage DC-grid," *IEEE Trans. Emerg. Sel. Topics Power Electron.*, vol. 7, no. 2, pp. 798–810, Jun. 2019.
[23] M. Abbasi and J. Lam, "A ∼99% η hybrid resonant/coupled ZCS-voltage-quadruplers MV SiC converter module for DC grid in wind systems," *IEEE Trans. Ind. Electron.*, vol. 68, no. 2, pp. 1231–1240, Feb. 2021.
[24] R. B. Beddingfield, A. M. Leary, R. Noebe, M. Nations, R. Bowman, and S. Bhattacharya, "Calculation of transformer leakage inductance by simplified flux path geometries," in *Proc. IEEE Energy Convers. Congr. Expo.*, 2022, pp. 1–8.

Yuge Yue received the M.Sc. degree in electrical engineering in 2023 from Shandong University, Shandong, China, where he is currently working toward the Ph.D. degree in power engineering, under the supervision of Dr. Guangzhu Wang.

His current research interests include ac/dc converters, dc/dc converters, and resonant converters.

Guangzhu Wang (Member, IEEE) received the M.Sc. degree in control engineering from the Harbin Institute of Technology, Harbin, China, in 1987, and the Ph.D. degree in power engineering from Shandong University, Jinan, China, in 2008.

Since 1987, he has been a Member of the Faculty of the School of Electrical Engineering, Shandong University. His current research interests include analysis and control of power converters, active power filters, multilevel converters, power cable fault location, and fault detection in distribution systems.

Wenjie Guo received the B.S. degree in electrical engineering and automation from the China University of Petroleum (East China), Qingdao, China, in 2016. He is currently working toward the M.S. degree in electrical engineering with the School of Electrical Engineering, Shandong University, Jinan, China.

His research interest includes the optimization and design of high-frequency transformers.